

ON THE EVALUATION OF ELASTIC PROPERTIES OF P. PINASTER AT THE GROWTH RING SCALE

Pereira, J.^{1,2}; Xavier, J.¹; Morais, J.¹; Lousada, J.¹; Pierron F.³

¹ CITAB, Universidade de Trás-os-Montes e Alto Douro, Portugal

² Departamento de Engenharia de Madeiras, Instituto Superior Politécnico de Viseu, Portugal

³ LMPF, Arts et Métiers ParisTech, France

ABSTRACT

In this work the identification of local elastic properties of maritime pine (Pinus pinaster Ait.) wood at the growth ring scale was investigated. Tensile tests through the radial direction were carried out on radial-tangential specimens. The strain fields over the gauge section were measured by digital image correlation. A balance between accuracy and spatial resolution was found out in order to assess the gradient strain fields generated by the heterogeneous cellular structure of the material. A segmentation technique based on image processing and analysis was implemented in order to split earlywood and latewood regions. The modulus of elasticity and Poisson's ratio of each earlywood and latewood layer were then determined. Effective mechanical properties were also evaluated and compared with reference to macroscopic properties and values from a mixture law. The results were found in good agreement.

1- INTRODUCTION

Wood and its derivative engineering products have been extensively used as building materials. Compared to other construction materials, wood is environmentally sensitive, it uses less overall energy, causes fewer, air and water impacts and plays an important role in global warming reduction by means of carbon consumption.

Xylem is a cellular biomaterial formed by softwood trees. It has a complex and heterogeneous anatomy which results from the ability of the tree to change its morphology, in response to changes on external conditions during its growing process. Therefore both physical and mechanical properties vary significantly within the stem and in particular along the radial direction (*R*) (Machado and Cruz, 2005, Xavier et al., 2009).

At the growth ring scale (1-10 mm), wood can be viewed as an inhomogeneous structure consisting of alternate layers of earlywood and latewood. In earlywood, the cells are characterised by thin walls and large lumens, whilst in latewood, the walls are thicker and lumens are smaller. Within an individual growth ring mechanical properties will follow that variation. It is relevant to know these sets of local properties since they can play an important role in applications such as fracture mechanics (Dourado et al., 2008) and dowel pin joints (Santos et al., 2009) for example. However, the material parameter characterisation at this scale of observation is challenging, namely because the generation of heterogeneous strain fields by the complex structure of the material itself. Nevertheless, this issue can be dealt with by taking advantage of the recent developments of full-field optical

techniques coupled with inverse identification methods (Grédiac, 2004).

The aim of the present work was to use the digital image correlation technique in order to measure the heterogeneous strain field (associated to the growth rings structure) generated when loading a rectangular specimen, oriented in the *RT* (radial-tangential) plane, by a tensile mechanical test. In a first approach, the closed-form solution of the tensile test (hypothesis of a uniaxial and plane stress approach) was directly used in order to determine the radial modulus of elasticity (E_R) and the Poisson's ratio in the *RT* plane (ν_{RT}) of the two main layers within the growth ring: earlywood and latewood. The natural polished surface of the material was used as textured pattern for the image correlation.

This paper presents some results of E_R and ν_{RT} associated to each earlywood and latewood layers, obtained from the local material mechanical response and analyse the relationship between density, measured by x-ray micro-densitometry and those elastic properties.

2-DATA REDUCTION

The mechanical model of the tensile test consists in applying a uniform tension load at the both ends of a thin rectangular specimen. For this simple configuration, a closed-form solution can be obtained, from which elastic properties can be determined as a function of the specimen geometry, the applied load and the strain state. Experimentally, this test can be carried out on a universal tensile machine, with controlled displacement rate. The applied load, P , can be measured by the load cell of the testing machine. The strain state at the gauge section of the specimen must be evaluated by a suitable technique. Thus, the modulus of elasticity and Poisson's ratio of a material can be determined, respectively, as

$$E_1 = \frac{P/A}{\varepsilon_1} \quad (1)$$

and

$$\nu_{12} = -\frac{\varepsilon_2}{\varepsilon_1} \quad (2)$$

where A is the cross-section area of the specimen, and ε_1 and ε_2 are the linear strains along the 1 and 2 axes of the specimen, respectively.

At the scale of observation, if the material can be accepted homogeneous, the hypothesis of a uniform strain state at the centre of the tensile specimen is usually assumed. Therefore, the strain state can be measured by punctual techniques such as strain gauges or extensometers. However, when the material is heterogeneous at the scale of the gauge region, a gradient strain field can be generated. This is the case of tensile tests at the growth ring scale, where gradient fields are generated by the heterogeneous cellular structure of the wood material itself. In this case, full-field optical techniques must be used in order to assess the gradient strain fields. These optical methods can be classified into white-light techniques (e.g., digital image correlation and grid methods) and interferometric techniques (e.g., speckle and moiré interferometry) (Grédiac, 2004). Conversely to punctual techniques, these techniques can provide full-field data and are contact-free. Due to its versatility and relative simplicity, the digital image correlation technique has been chosen. The spatial resolution of this technique is physically limited by the pixel resolution of the CCD (Charge-coupled device) camera to be used. However, this technique can be easily coupled with a universal testing machine (there is no need of anti-vibration table or lasers) and requires relatively simple specimen preparation than other counterpart methods.

3–DIGITAL IMAGE CORRELATION

The underlying idea of the digital image correlation (DIC) method is to tracking a set of points (pixels) between two images, taken before and after the application of a given deformation (Fig. 1). In the implementation of the DIC method, a virtual grid is created to slit the reference (undeformed) image into a set of evenly spaced correlation windows, which size (number of pixels) must be chosen by the user in a compromise between spatial resolution and accuracy. An independent value of the displacement is computed over each subset in order to obtain full-field measurements. Thus, the size of the subset will define the displacement resolution, *i.e.*, the distance between adjacent independent measurements. A set of pixels, rather than an individual pixel, is used to define each subset target because this will uniquely identify their mapping into the deformed image. In the evaluation of the similarity among reference and deformed subsets, a suitable correlation function must be predefined. This will determine the new position of the deformed subsets, thus, yielding the in-plane displacement vector of each subset by the difference between undeformed and deformed coordinates. Further details about the DIC method can be found in a recent survey by Pan et al. (2009).

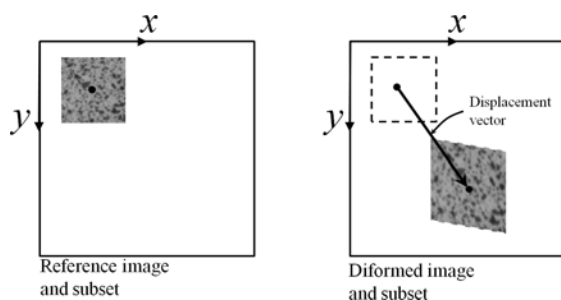


Fig 1 – Schematic representation of the digital image correlation method.

4–EXPERIMENTAL WORK

4.1 – Material and specimens

The wood material used in this work came from an 80-year old maritime pine (*Pinus pinaster* Ait) tree, which was grown in the mid-central region of Portugal. Plain-sawn boards were cut from logs and dried in a kiln in order to reach a moisture content of about 12%. Parallelepiped specimens oriented along the *RT* plane and with dimensions of 50(*R*)x7(*T*)x3(*L*) (mm³) were cut from the central plain-sawn board at the breast height of the stem (Fig. 2).

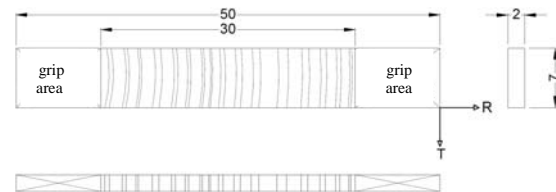


Fig 2 – Specimens geometry and dimensions.

The temperature and the relative humidity during testing were around 23°C and 50%, respectively. Specimen dimensions were measured before testing.

4.2 – Micro-densitometry measurements

For *Pinus pinaster*, wood density variation inside the growth rings is normally considered between 0.4 and 0.9 g/cm³ (Lousada, 2000). It results from the differences between latewood and earlywood layers, namely the ratio between cellular wall volume and the overall cellular volume.

X-ray micro-densitometry measurements were carried out to assess the local density of wood, as well as the respective dimensions and fractions of the earlywood and the latewood layers within the growth rings, as described in Lousada (2000). Samples with nominal dimensions of 3(*L*)X5(*T*) (mm) and length equal to the local radius of the central board were used. The radial density profile was measured

On the evaluation of elastic properties of p. pinaster at the growth ring scale

with a spatial resolution of 0.1 mm. In the calculations, for the segmentation of layers within individual growth rings, the density threshold of 0.650 g/cm^3 was chosen. This value was considered in spite of the evidence (Lousada, 2000) that it split a high amount of transition wood to the latewood percentage, turning the earlywood density less accurate on the determination of the mean density value.

4.3 – Tensile tests

The tensile mechanical tests were carried out on an Instron 5848 MicroTester testing machine under displacement control at a rate of 0.05 mm/min (Fig. 3). The load was measured by a 2 kN load cell. Images were grabbed during the tests with an acquisition frequency of 1.0 Hz.



Fig 3 – Set-up of the tensile test and image acquisition.

4.4 – Full-field measurements

4.4.1 – Surface preparation: textured pattern

The DIC method assumes that the imaged surface has a textured pattern from which the diffusely reflected light intensity will vary continuously and with a suitable contrast. Either the surface of the material has naturally such a textured pattern or it can be created by painting (*e.g.*, spray or airbrush paint, toner powder deposit or lithography). In this work, the natural texture of a specimen surface was used as a carrier for the material deformation analysis. The surface of interest ($7 \times 9 \text{ mm}^2$, Fig 4) was polished by using sandpaper with granulometries between P120 and P400. At the scale of the growth rings, the natural cellular structure of the wood could be conveniently used as carrier for the

material deformation analysis by the DIC method (Fig. 4).

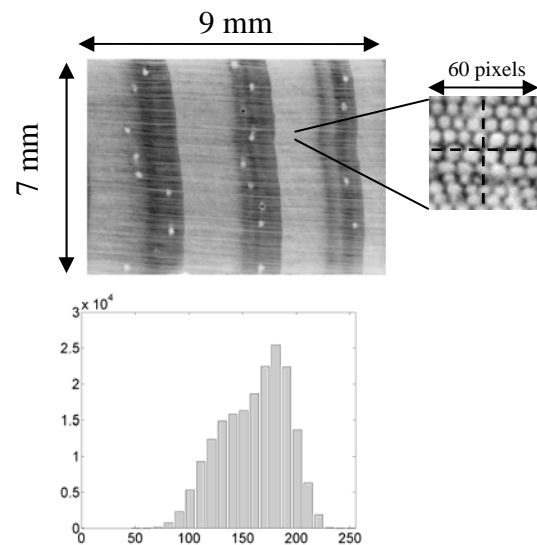


Fig 4 – Cellular textured surface of wood used in the DIC method.

4.4.2–Set-up and measuring parameters

The digital image correlation code Aramis 6.02 from GOM® (www.gom.com) was used in this work. An 8-bit Baumer Optronic FWX20 camera (resolution of 1624×1236 pixels, pixel size of $4.4 \mu\text{m}$ and sensor format of 1/1.8") was chosen for image grabbing (Fig. 3). In order to achieve the desired magnification at the growth ring scale, a Nikon AF Micro-Nikkor 200mm f/4D IF-ED was coupled to the optical system.

The camera-lens optical system was positioned with regard to a specimen mounted into the mechanical set-up. A level ruler and a laser pointer were used to guarantee a correct alignment. The measuring distance (defined between the specimen's surface and the support of the cameras) was set about 400 mm (Table 1). The camera was then focused, opening the lens aperture to $f/2.8$. For testing, however, the aperture of the lenses was slightly closed ($f/11$) in order to improve the depth of field. The shutter time was set to 50 ms (cross-head displacement rate of 2 mm/min and the size of the camera unit cells of $4.4 \mu\text{m}$). The light source was finally adjusted

in order to guarantee an even illumination of the specimen surface and to avoid over-exposition (*i.e.*, the saturation of pixels over the field of view).

In the DIC method, an independent measurement of the displacement is achieved at each subset splitting the reference image. The size of these facets will define the displacement spatial resolution of the method, and must be chosen in a compromise taking into account the accuracy of the method. The facet step (*i.e.*, the distance between adjacent facets) can also be set either for controlling the total number of measuring points over the region of interest or for enhancing the spatial resolution by slightly overlapping adjacent facets. Typically, a large correlation window (facet size) will improve the accuracy of the measurements but, in counterpart, a coarse spatial resolution will be obtained (Lecompte et al., 2006). In this work, a facet size of 30×30 pixels was chosen, attending to the size of the region of interest, the optical system (magnification) and the quality of the texture pattern (Table 1). The facet step was also set to 30×30 pixels (Table 1), in order to have statistically uncorrelated measurements.

The in-plane displacements were then numerically differentiated, over a region of 3×3 macro-points (Table 1), in order to determine the strain field need for the material characterisation problem.

Table 1 – Measuring parameters: Aramis - GOM.

CCD Camera:	8-bit Baumer Optronic FWX20 (1624×1236 pixel)
Lens:	Nikon AF Micro-Nikkor 200mm f/4D IF-ED
Working distance:	400 mm
Conversion factor:	$6 \mu\text{m} \cdot \text{pixel}^{-1}$
Acquisition frequency:	1.0 Hz
Facet size and step:	30×30 pixels ($180 \times 180 \mu\text{m}$)
Local differentiation:	3×3 macro-pixels

4.4.3 – Measuring resolution: static tests

A static test was performed taking several images without deforming the specimen (*i.e.*, motionless test). Since no deformation is applied during image acquisition, the displacement fields calculated by digital image correlation will represent a noisy signal. The statistical analysis of these fields will allow assessment to the accuracy of the measurements. This study is summarised in Fig. 5. The U_X displacement field typically obtained from such test is shown in Fig. 5a). This field represents a Gaussian noise signal which histogram can be seen in Fig. 5b). The standard deviation over the full-field displacements was calculated. This result is presented in Fig. 5c) where, a displacement resolution lower than $1 \mu\text{m}$ is typically obtained. The same kind of analysis was performed over the computed strain maps (Fig. 5d). A standard deviation of the order of 10^{-4} was obtained, which represents a strain resolution usually achieved with the DIC method. This resolution is still suitable for measuring the strain field in the elastic domain. These results validate the measuring procedure in applying the DIC method to the wood analyses at the growth ring scale.

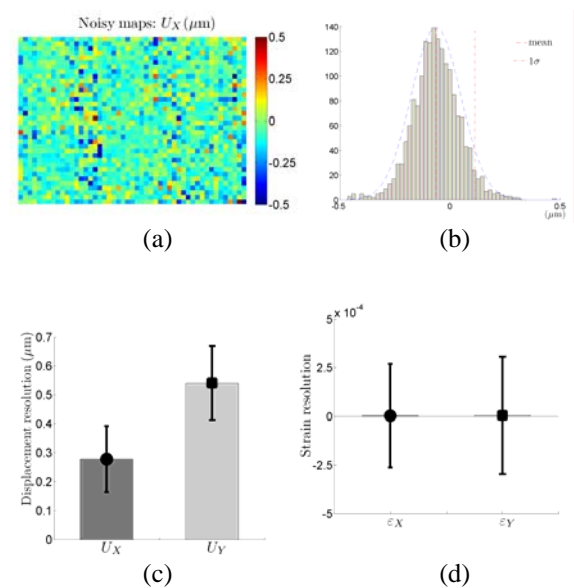


Fig 5 - Static tests: (a) U_X displacement; (b) histogram; (c) displacement resolution; (d) strain resolution.

5- RESULTS AND DISCUSSION

5.1 – Global mechanical response

The data measured during the tensile test are the applied load and the strain state at the gauge region of the specimen. An example of the strain field measured over the gauge region by the DIC method is shown in Fig. 6 (load = 50.4 kN). As it can be seen heterogeneous strain fields are actually obtained, following the heterogeneity of wood at the growth ring scale (see Fig. 4). An effective (average) strain was evaluated from these maps. Thus, a global stress-strain curve was obtained (Fig. 7), assuming a uniaxial and plane stress approach.

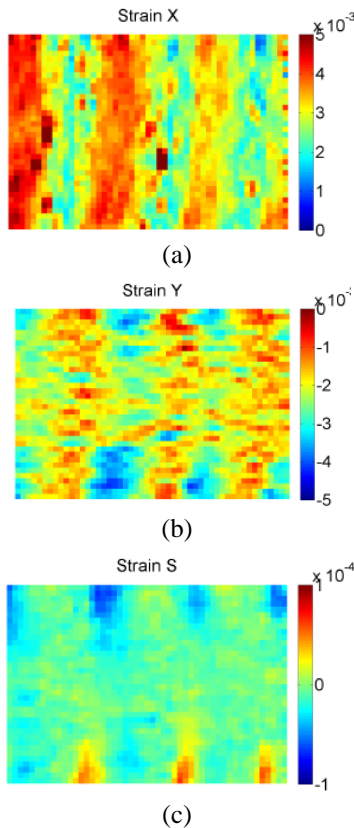


Fig 6 – Strain-fields (load = 50.4 N): (a) ε_X ; (b) ε_Y ; (c) ε_S .

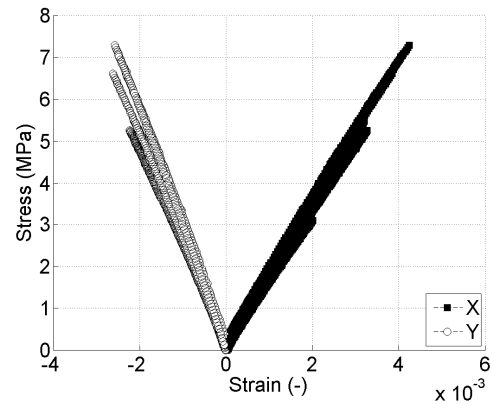


Fig 7 – Global (effective) stress-strain curve (X-radial direction; Y-tangential direction).

5.2 – Local mechanical response

The heterogeneous strain fields measured at the growth rings scale were further processed in order to assess to the local mechanical response of each earlywood and latewood constituents. For that purpose, image processing and analysis were performed on the images of the wood structure (*i.e.*, the same images used for the DIC analysis) in order to segment each constituent region. This procedure consisted in two main steps: segmentation and morphological operations. Firstly, each image was split in order to roughly separate individual growth rings, observed over the field of view. Secondly, a single thresholding technique was applied over the obtained sub-images in order to define each earlywood and latewood layers. This segmentation step was, however, insufficient to correctly obtain segmented regions due to the rather complex light intensity distribution of the heterogeneous cellular structure of the material. Therefore, an additional step was implemented based on morphological operations (erosion and dilatation). In conclusion, typical segmented regions are shown in Fig. 8(a). This allowed the definition of earlywood and latewood masks. These segmented regions were then used in order to segment the strain fields as shown in Fig. 8(b). Based on this segmentation, local stress-strain curves

were then obtained for each earlywood and latewood layers, as represented in Fig. 9. As it can be seen, for a given level of applied stress, the latewood layer (Fig. 9.a) has a lower deformation (*e.g.*, ε_X) than the earlywood one (Fig. 9.b). This is consistent with the variation of the cellular structure within the growth rings.

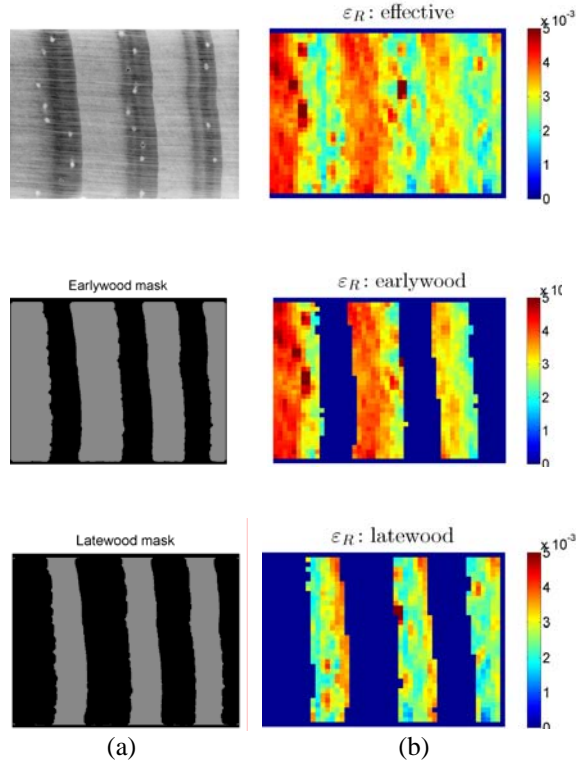


Fig 8 – (a) Growth rings structure and segmented earlywood and latewood regions; (b) ε_R strain field and segmented ε_R over the earlywood and latewood regions.

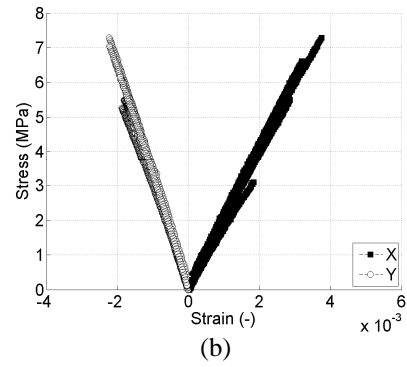
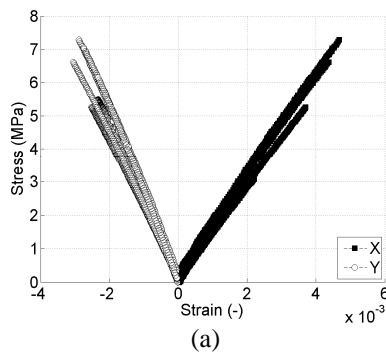


Fig 9 – Local stress-strain curve: (a) earlywood, (b) latewood (X-radial direction; Y-tangential direction).

5.3 –Elastic properties at the growth ring scale

From the global (Fig. 7) and local (Fig. 9) stress-strain curves, effective, earlywood and latewood elastic properties were determined by linear least-squares regression. This study is summarised in Table 2, where the E_R (Eq. 1) and the ν_{RT} (Eq. 2) elastic properties, along with the mean density (ρ) of the specimen (measured from X-ray micro-densitometry, Section 4.2), are reported. The ratio of densities between early and late woods is about 2, which is a typical value for this species (Lousada, 2000). It is interesting to see that the scatter (measured by the coefficient of variation CV) associated to the elastic properties is rather small. The mean value of E_R is consistent with what one could expect from the stress-strain curves (Fig. 7), *i.e.*, the properties of earlywood and latewood are statistically different, being the latewood tissue stiffer than the earlywood one. However, the same mean value was statistically obtained for ν_{RT} , showing that globally the Poisson's ratio can be assumed constant within the growth ring. The effective elastic properties determined from the measurements at the growth rings scale were finally compared with some reference values. The elastic properties reported from radial tensile tests carried out at the macroscopic scale (Pereira, 2005), as well as an estimation of the modulus of elasticity determined by a mixture law on a

On the evaluation of elastic properties of p. pinaster at the growth ring scale

series model were chosen as references. The following mixture law was used

$$E_R^{effective} = \frac{E_R^{EW} \times E_R^{LW}}{E_R^{EW} f^{EW} + E_R^{LW} f^{LW}} \quad (3)$$

where $f^{LW} = 45\%$ represents the percentage of latewood (LW) in the growth ring, measured from the X-ray microdensitometry. This study is summarised in Fig. 10. As it can be seen the E_R (Fig. 10.a) and the ν_{RT} (Fig. 10.b) effective properties determined at the meso scale are in good agreement with regard to the reference values.

Table 2 – Measuring parameters: Aramis - GOM.

	Effective	Earlywood	Latewood
ρ (gcm ⁻³)	0.70	0.455	0.976
E_R			
MEAN (GPa)	1.74	1.59	2.00
CV (%)	3.5	4.8	3.0
ν_{RT}			
MEAN (GPa)	0.641	0.646	0.631
CV (%)	5.6	6.4	4.8

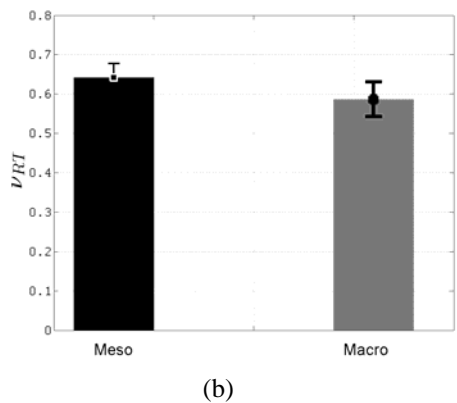
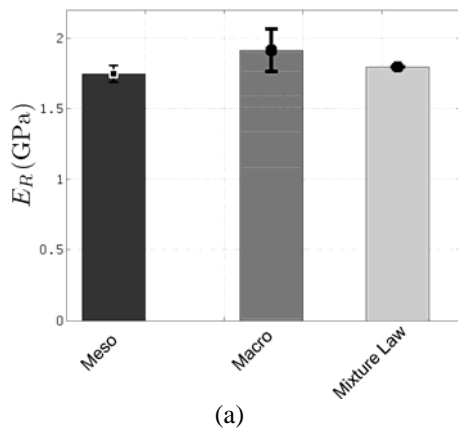


Fig 10 – Comparison of effective elastic properties of *Pinus pinaster*: (a) modulus of elasticity E_R ; (b) Poisson's ratio ν_{RT} .

6 – CONCLUSIONS

In this work tensile tests were carried out at the growth ring scale in order to assess local elastic properties of maritime pine (*Pinus pinaster* Ait) wood. Heterogeneous strain fields associated to the earlywood and latewood layers within the growth rings were measured by digital image correlation, with a suitable balance between spatial resolution and accuracy. The polished natural surface of wood was used as textured pattern for the image correlation. Local elastic properties (E_R , ν_{RT}) of early and late woods of *Pinus pinaster* wood were determined, assuming a uniaxial and plane stress approach. The results are consistent with the variation of the cellular structure within the growth rings. Moreover, effective properties are in good agreement with reference values determined from tensile tests at the macroscopic scale on clear wood specimens, as well as from a mixture law.

A further investigation is currently undergoing in order to identify the spatial variation of the four RT elastic properties (E_R , E_T , ν_{RT} , G_{RT}) by a single tensile test, coupling full-field optical techniques with suitable inverse identification methods.

ACKNOWLEDGEMENTS

We would like to thank the Foundation for Science and Technology (FCT) for the Ph.D. scholarship of J. Pereira and the financial support by the European Science Foundation and MCTES - through the POPH-QREN - Typology 4.2.

REFERENCES

Dourado, N., Morel, S., de Moura, M.F.S.F., Valentin, G., Morais, J. Comparison of

- fracture properties of two wood species through cohesive crack simulations. *Composites Part A: Applied Science and Manufacturing* 39(2): 415-427, 2008
- Grédiac, M. The use of full-field measurement methods in composite material characterization: Interest and limitations. *Composites Part A: Applied Science and Manufacturing* 35(7-8):751-761, 2004
- Grédiac, M., Pierron, F., Avril, S., and Toussaint, E., The virtual fields method for extracting constitutive parameters from full-field measurements: a review, *Strain*, 42(4):233–253, 2006
- Lecompte, D., Smits, A., Bossuyt, S., Sol H., Vantomme, J., Van Hemelrijck, D., Habraken, A.M., Quality assessment of speckle patterns for digital image correlation. *Optics and Lasers in Engineering*, 44(11): 1132-1145, 2006
- Lousada, J.L. Variação fenotípica e genética em características estruturais na madeira de *Pinus pinaster* Ait. PhD thesis, Universidade de Trás-os-Montes e Alto Douro, Vila Real, Portugal, 2000. (in Portuguese)
- Machado, J.S. and Cruz, H.P., Within stem variation of Maritime Pine timber mechanical properties, *Holz als Roh - und Werkstoff*, 63(2):154–159, 2005
- Pereira, J.L., Comportamento mecânico da madeira em tracção nas direcções de simetria material. M.Sc. Thesis, University of Trás-os-Montes e Alto Douro, Vila Real, 2005
- Pan, B., Qian, K., Xie, H., Asundi, A. Two-dimensional digital image correlation for in-plane displacement and strain measurement: a review. *Measurement Science and Technology* 20(6): 062001 (17pp), 2009
- Santos, C.L., de Jesus, A.M.P., Morais, J.J.L., Lousada, J.L.P.C. Quasi-static mechanical behaviour of a double-shear single dowel wood connection. *Construction and Building Materials* 23(1): 171-182, 2009
- J. Xavier, J. Pereira, J. Morais, F. Pierron, J. Lousada: On the estimation of elastic properties of wood at the growth ring scale. COST FP0802 Experimental and Computational Micro-Characterization Techniques in Wood Mechanics, Vienna, Austria, 11-13 May, 2009